Estimation of Permeability, Porosity and Rock Compressibility Properties using Digital Rock Analysis Technique for a Heavy Oil Unconsolidated Sandstone Offshore Brazil*

M.F. de Siqueira[1], F. Silva[1], M.D. Marsili[2], P.S. Rocha[2], A. Kronbauer[2], C. Sisk[3], A. Grader[3], J. Toelke[3], and A. Jordan[3]

Search and Discovery Article #30587 (2018)**
Posted November 12, 2018

*Adapted from extended abstract based on oral presentation given at AAPG 2018 Annual Convention & Exhibition, Salt Lake City, Utah, United States, May 20-23, 2018
 DOI:10.1306/30587deSiqueira2018

[1]Ingrain Brasil, Rio de Janeiro, Brazil (milena.siqueira@halliburton.com)
[2]Queiroz Galvão Exploração e Produção S.A., Rio de Janeiro, Brazil
[3]Ingrain Inc., TX, United States

Abstract

Mechanical, storage, and transport rock properties are fundamentally important in the characterization of oil and gas reservoirs. Traditionally, these properties are obtained by conventional well logging techniques, seismic inversion, and laboratory tests from cores, sidewall cores, plugs, and rock cuttings. However, for unconsolidated rocks, conventional recovery techniques of rock samples and performing laboratory tests are subject to failure at all stages of the process. Because of the unconsolidated nature of the rock, fractures are created by the expansion of the gas evolved from the oil inside the rock during the recovery of the material to the surface at the well site. In addition, there are challenges with taking physical plugs from the surface core material, including the cleaning and conditioning required for traditional physical laboratory testing. In these types of scenarios, digital simulations using X-ray microtomography is one of the techniques that have been used to address these difficulties. From imaging the rock samples using computed microtomography (micro-CT), a 3D image of the grain and pore system is created, and with new equipment and workflows, the rock compressibility properties can be measured. This study focuses on the development of a rock compressibility methodology using digital images to quantify key reservoir properties, including porosity, absolute permeability, and pore compressibility, that are important for the field development planning and management, reservoir performance monitoring, and reserves assessment. This paper describes the equipment designed to enable scanning the rock samples under different hydrostatic pressures using the latest micro-CT equipment, and then taking these scans and calculating the change in porosity, permeability, and other properties. The results are compared to other available sources, including openhole logs with in-situ porosity, along with Newman's (1973) work for rock compressibility assuming uncemented sandstone.

Introduction

Significant volumes of heavy oil with high viscosity have been discovered offshore Brazil. Offsetting the difficulties encountered in the production of these crudes is that some of these fluids are stored in excellent quality reservoir rock, for example, high porosity and permeability, providing an opportunity for the economic exploitation of these accumulations. Although these rocks are of good quality, a large majority of the sandstone rock fabric is unconsolidated. Consequently, they are difficult to sample, handle, and test in the laboratory to determine their properties.

The rock properties are fundamentally important to characterize oil and gas reservoirs, affecting the various disciplines involved in the development of production of a deposit, including reservoir engineering, development geology, seismic, drilling, and completion. The key rock properties include permeability, porosity, rock compressibility, relative permeability, capillary pressure, particle size distribution, compressional velocity, shear rate, elastic modulus, shear modulus, and cementation factor.

Traditionally, these parameters are obtained by conventional logging techniques, seismic inversion, and laboratory tests from samples, side, and rock cuttings samples. However, in the scenario of unconsolidated rocks, conventional rock sample recovery techniques and performing laboratory tests are subject to failure at all stages of the process. By the very nature of unconsolidated rocks, the recovery of the core is impaired, often crumbling during the recession. When retrieved, the rocks are usually changed by fractures created by the expansion of solution gas evolved from the oil inside the rock. There are also additional difficulties in plugging these rocks, cleaning, and conditioning for testing. Laboratory test results must be evaluated with the consideration that the rock structure has been altered.

Digital simulations using X-ray microtomography is a technique that has been used to overcome the difficulties posed by this scenario. From imaging the rock samples using computed microtomography (micro-CT), a 3D image of the grain and pore system is created, and the petrophysical properties are calculated mathematically from physical principles. Consequently, several bottlenecks can be overcome in determining properties of these rocks. Several publications, including Dvorkin et al. (2008) and Grader et al. (2010), have shown the validity of this technology to compare results of laboratory tests with results obtained by digital petrophysics.

This research focuses on the study of the physical compression combined with digital rock analysis to estimate the sensitivity of the rock with the increase in net effective stress. This research investigated methodologies to approximate the compressibility of the rock related to the reduction in porosity, an increase in the pore volume compressibility (cf), and an estimate of the decrease in permeability.
Sampling material used in this research came from Atlanta field; a post-salt oil field located 185 km off the coast of Rio de Janeiro. In accordance with Marsili et al. (2015), the field was discovered in 2001. The appraisal operation, begun the same year, included a deviated well to test the Eocenic sandstones. A cased hole gravel pack completion was installed. The 90 m interval tested showed an unconsolidated sandstone, with high porosity (36%) and high permeability (4 to 6 Darcy). However, the oil is heavy and viscous (14°API and 228 cP in reservoir conditions), and very acidic (TAN = 10 mg KOH/g).

Method

This section describes the workflow and procedure for the physical compression tests integrated with digital technology. The goal is to compress the sample to the point at which it becomes load bearing. At each confining stress, the samples are scanned, and the properties are determined, such as porosity, permeability, and later, rock compressibility.

This project uses a proprietary compression chamber to scan rock samples under different net hydrostatic effective stresses at a sufficiently high resolution to define the pore and grain structures. Figure 1 shows a schematic of the experiment. The physical compression, using digital simulation, consists of 5-mm diameter samples that are hydrostatically compressed in a drained state (Figure 1 (a)). They are in a titanium X-ray transparent vessel and scanned at 2 to 4 net effective stresses (20, 1250, or 1500 psig; in some cases, 500 and 2000 psig are used in addition to the first two) (Figure 1(b)).The rock samples are imaged at approximately 4-micron resolution, and these 3D images serve as the starting platform for digital rock analysis.

Four plugs from Atlanta field were selected for physical compression, and two sub-samples were extracted from each plug. Table 1 summarizes the sub-sample settings from the analysis under physical compression high and low pressure.

Digital Conditioning

The expanded or damaged cores as received at the surface have higher porosity and permeability values than in the reservoir. The additional porosity is manifested by large pores that were created when grains moved because of pore pressure relief during lift. The entire core swells in volume. In some cases, these large pores align to form planar features that may strongly affect permeability.

To provide results better correlated with reservoir condition, the digital conditioning process was developed. This process includes two main steps:

- Identify the expanded pores.
- Impress on these pores a grain structure taken from the same digital volume.

The typical result from the conditioning process is that some of these extra pores are filled with grains with a similar size distribution of the original rock. Figure 2 shows a single slice in axial view illustrating the digital pore and grain structure before and after digital conditioning. The process of impressing the 3D grain structure on the pore is random in nature. It is not likely that compressing the plugs physically will return the rock to its original reservoir condition. The conditioning process is not a perfect answer to correcting the results derived from expanded cores. However, digital conditioning does move the rock grain structure closer to its original state so that both static and dynamic properties can be estimated with increased confidence. Figure 3 shows a comparison between two subsamples extracted from different positions of the same plug (example plug 8-101) PRE and POST compression and before and after digital conditioning.

Porosity

Porosity is a fraction of the bulk volume that is not occupied by solid. Helium porosity detects the connected porosity in a rock sample. Although geologic settings exist that have isolated porosity that even helium cannot detect, this porosity is rare. In digital rock analysis, at a given imaging resolution, helium porosity is divided into two parts: the directly-detectable-porosity (DDP) that can be segmented out or separated from the rest of the solids in the plug, and the sub-resolution porosity that cannot be segmented out.

As the sample size decreases and the resolution increases, the fraction of the DDP increases. The DDP is a simple ratio of the number of the segmented porosity voxels to the total number of voxels that encompass the bulk volume. It is the same base definition of experimental porosity.

The non-directly-detectable-porosity (NDDP) can be estimated using CT averaging methods that have been used in digital simulations for years. This method is based on the linearity of the recorded CT values with mineral mixtures including porosity. This method requires the knowledge of the mineralogy of the rock sample if it consists of more than one mineral.

Absolute Permeability

Permeability is computed by simulating the flow of fluid directly through the pore structure that is defined through the segmentation process of the 3D digital rock. The simulation method used, Lattice Boltzmann (LB), approximates Navier-Stokes single-phase flow. This technique subjects the digital rock to the same conditions as performed experimentally. A pressure decrease is applied across the digital sample, and the resulting stabilized flow rate is computed. The ratio of the rate to the pressure decrease is directly related to permeability.

Rock Compressibility

Rock compressibility was estimated using the total porosity and net confining pressure applied during the physical compression test using digital simulation. The rock compressibility is defined as (Fatt, 1958):

$$c = -\frac{1}{V_B}\frac{\partial V_B}{\partial P}$$

The pore volume compressibility is defined as:

$$c_f = -\frac{(\phi_2 - \phi_1)}{\phi_1} \cdot \frac{1}{(P_2 - P_1)}; \qquad P_2 > P_1$$

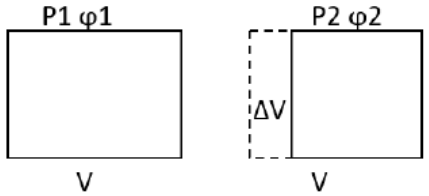

Where,

ϕ_1 = Total porosity at pressure P1 (low pressure)
ϕ_2 = Total porosity at pressure P2 (high pressure)
P_1 = pore pressure (atmospheric pressure – psig)
P_2 = lithostatic pressure (psig)

To calculate the effective compressibility using the results of the digital rock results before and after the hydrostatic compression during the scan, the following assumptions were made:

1. The equipment can repeat the scans with the same configuration and repeat the same resolution. Thus, when setting a volume of voxels, a physical volume for the calculation of material properties is also set.
2. Segmentation of porosity between scans under different pressure conditions is sufficiently accurate to capture pore system differences before and after compression.
3. The grains will have a solid incompressible behavior under the applied pressure differential, and the volume changes will be attributable to the compressibility of the pores.
4. Compressibility was calculated in samples both before and after digital conditioning.

Results

Figure 4 shows sub-sample 8-101-1 depth 2348.18 m pre- (P0000) and post- (P1250) compression CT data at the same slice position. The two scans are taken at the same Z level on the scanner, and the bottom of the sample does not move. During the compression test, the Z direction is “compressed” from the top and compresses toward the fixed bottom. Therefore, the middle of the POST scan is lower physically than in the PRE scan. Relative to the base of the sample, the grains move downward. The large grain in image (a) looks different from the same grain in image (b) because it is not in the same elevation. In this case, the shift is by 22 slices. Image (c) looks similar in shape to the same grain in image (b).

Figure 5 shows the PRE and POST compression CT data on the XZ view with a clear shift on the grain positions after the compression test. The orange lines on the edges are used to cut a digital sample that maximizes the same populations of grains in the PRE and POST scans.

A low-resolution scan of the entire sub-sample was taken before and after applying the confining pressures. Figure 6 shows one single slice of the entire scan at 12 microns per voxel of sub-sample 4-3-2 depth 2375.85 m. The single slices show scans at low pressure (20 psig) and high pressure (1,500 psig). Note the reduction in area occupied by grains in the figure on the right (P1500). The black spaces between the grains represent a vapor phase (air at the time of the experiment). There is significant air saturation, even at the high confining pressure. This ensures that the pore pressure is low and that the increase in confining pressure can be considered to translate to net effective stress.

The results of the first test applying low pressure 20 psig and high pressure 1,250 psig for sub-sample 8-101-1 depth 2348.18 m show that the porosity changes before and after the compression could be associated with the air saturation. The computed total porosity of sub-sample 8-101-1 depth 2348.18 m at low pressure was 35.1% with 1.7% associated with the air porosity shown on Figure 7. After applying the high pressure, the total porosity decreased to 33.2%, which is a difference of 1.9% before and after the hydrostatic compression.

The relationship of the air, oil, and grains was also analyzed on the second set of tests, including the four different pressures for sub-sample 4-3-2 depth 2375.85 m. Figure 8 shows segmented CT slices in which grains are shown in red, air in blue, and oil in green. When pressure stages are increased, smaller differences in the distribution of the oil in the pore space is captured. This conclusion does not follow for air volume, however; in this case, increasing pressure modifies the air volume fraction under consideration and reduces the percentage of air in the pore space.

Table 2 shows the quantification of the segmented pore space capturing air and oil. Figure 8 (a) shows porosity, oil saturation, and air saturation at four confining stresses, and Figure 8 (b) shows the four slices in segmented mode and demonstrates the reduction of the air saturation (blue). As shown, the oil saturation increases initially to 200 psig as more oil-surrounded grains are moved into the scan volume. However, after the grains become strongly load bearing, the oil and the air saturation decrease along with the overall porosity.

Table 3 summarizes the total porosity and absolute permeability computed for hydrostatically compression CT analysis under different levels of net confining pressure for all four selected plugs from the Atlanta field. The computations were performed for the pressures steps 20, 1,250, and 1,500 psig.

It is not a trivial process to determine whether or not a sample requires digital conditioning. The 3D pore space must be investigated. If tunnels and extremely large pores as previously described exist, then it can be applied. Sometimes, however, it is not so obvious. A test must be performed in which the pore must be selected and passed by morphological mathematic tools to map the entire pore structure and then decide whether or not conditioning can be applied. Plugs selected for digital conditioning in this investigation were: 4-3 depth 2375.85 m sub-sample 1 and 2 (4-3-1 and 4-3-2), 8-101 depth 2348.18 m, sub-sample 1 and 2 (8-101-1 and 8-101-2), and 4-80 depth 2394.98 m, sub-sample 1 and 2 (4-80-1 and 4-80-2). All of the samples were under low pressure (20 psig) and high pressure. Because of the condition of the sub-sample, plug 8-1 depth 2323.43 m does not require digital conditioning. Figure 9 shows an example of the decrease in porosity and permeability after applying digital conditioning. The trend plotted was acquired using digital subdivision trend workflow as described by Proctor et al. (2015).

Figure 10 shows the analysis of the digital rock volumes under hydrostatically compressed stages for the sub-samples from the Atlanta field. The effective rock compressibility was computed using the total porosity and the effective net pressure applied during the physical compression; results displayed are related to the results reported by Newman (1973) for unconsolidated sandstone.

Conclusions

The following conclusions can be drawn from this study:

- Digital rock analysis, when applied correctly, can provide a vital source of relevant measurements for formations that have unconsolidated sandstone with heavy oil.
- The damage created during the recovery of the rocks to the surface and after they are at the surface can be identified using digital rock analysis.
- The workflow using in this project enabled improved estimation of porosity, permeability, and rock mechanic information.
- The specially designed tool and workflow used in this project successfully increased the pressure to that of the reservoir condition; to restore the porosity and permeability to the original in-situ values, the digital conditioning technique must be applied to digitally restore the grains to their original 3D position. Physical compression at the microscale helps to define some of the compressibility issues, but does not restore the porosity (and consequently the permeability) to the values in the reservoir. Digital conditioning is still suggested as one of the viable methods to obtain petrophysical properties that are closer to the values in the reservoir.

Acknowledgments

The authors acknowledge Queiroz Galvão Exploração e Produção S.A. (QGEP) for their support to perform this research and Barra Energia do Brasil Petróleo e Gás Ltda together with QGEP, and Halliburton for the permission to publish this paper. The Agência Nacional do Petróleo, Gás Natural e Biocombustíveis (ANP) is also acknowledged for providing financial support and a national system of encouraging the use of new technology coupled with training of Brazilians.

References Cited

Dvorkin, J., M. Armbruster, C. Baldwin, Q. Fang, N. Derzhi, C. Gomez, A. Nur, and Y. Mu, 2008, The Future of Rock Physics: Computational Methods Versus Lab Testing: First Break, v. 26/9, p. 63-68.

Fatt, I., 1958, Pore Volume Compressibility of Sandstone Reservoir Rocks: Journal of Petroleum Technology, v. 10/3, p. 64-66. SPE-970-G, http://dx.doi.org/10.2118/970-G.

Grader, A., Y. Mu, J. Toelke, C. Baldwin, Q. Fang, G. Carpio, B.A. Stenger, T. Al-Dayyani, and M.Z. Kalam, 2010, Estimation of Relative Permeability Using the Lattice Boltzmann Method For Fluid Flows, Thamama Formation: Presented at the Abu Dhabi International Petroleum Exhibition and Conference, Abu Dhabi, UAE, 1-4 November, SPE-138591-MS, https://doi.org/10.2118/138591-MS.

Marsili, M.D., G.G. de Góes Monteiro, C.A. Pedroso, S.J.A. Neto, I. de Almeida Ferreira, P.S. Rocha, M. Rausis, and V. Branco, 2015 Atlanta Field: Developing Heavy and Viscous Oil in a Challenging Environment: Presented at the Offshore Technology Conference, Houston, Texas, USA, 4-7 May, OTC-25813-MS, https://doi.org/10.4043/25813-MS

Newman, G.H., 1973, Pore-Volume Compressibility of Consolidated, Friable, and Unconsolidated Reservoir Rocks under Hydrostatic Loading: Journal of Petroleum Technology, v. 25/2, p. 129-134, SPE-3835-PA. https://doi.org/10.2118/3835-PA.

Proctor, J., P.H. Vieira de Luca, G.A. Pimentel, C. Sisk, M. Oliveira, A. Huber, R. Sungkorn, J.L.A. Alonso, R.P. Jiménez, and V. Silos, 2015, Porosity and Permeability Upscaling in a Lagoa Salgada Stromatolite and Codó Formation Stromatolite: Presented at the 14th International Congress of the Brazilian Geophysical Society & EXPOGEF, Rio de Janeiro, Brazil, 3-6 August, p. 788-792, https://doi.org/10.1190/sbgf2015-154

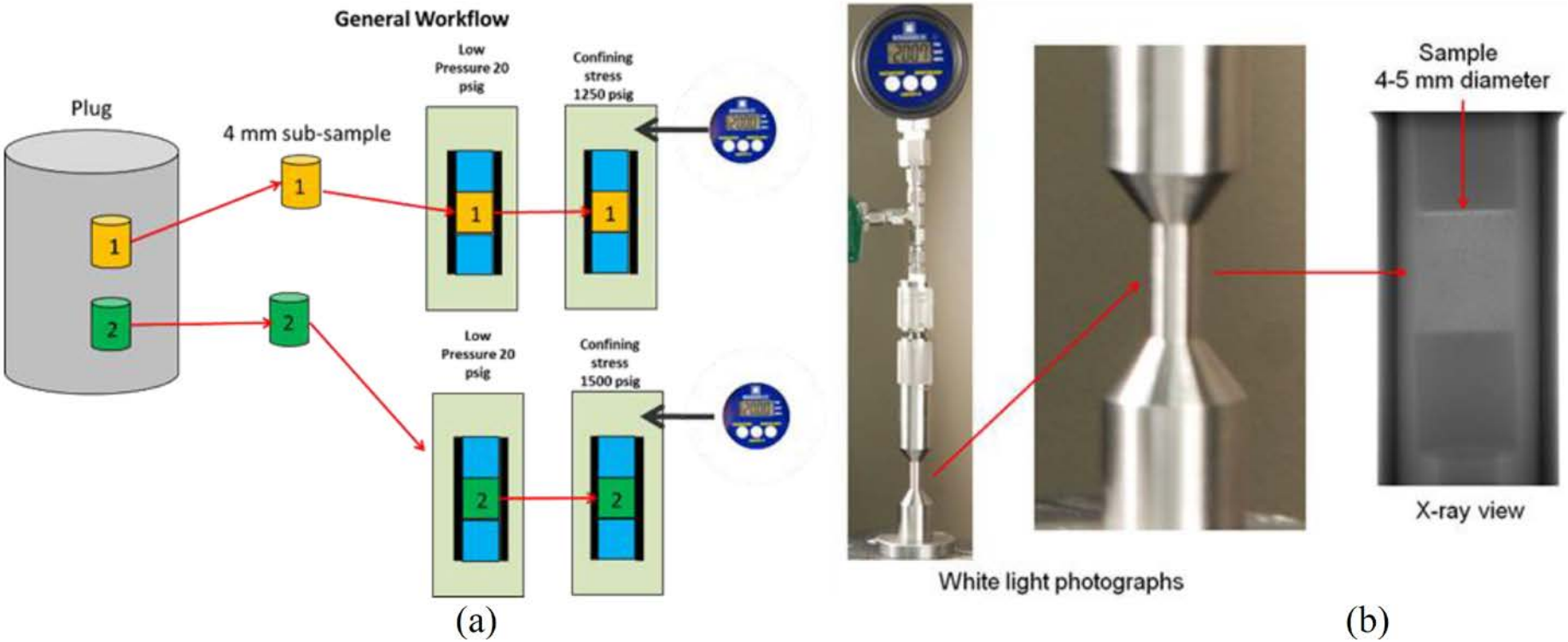

Figure 1. Physical compression – (a) General workflow with schematic of the sub-sample position extracted from the plug and then positioned on the confining chamber for pre- and post-scans; (b) Confining compression chamber example with white light photograph and X-ray view of the sub-sample inside of the chamber.

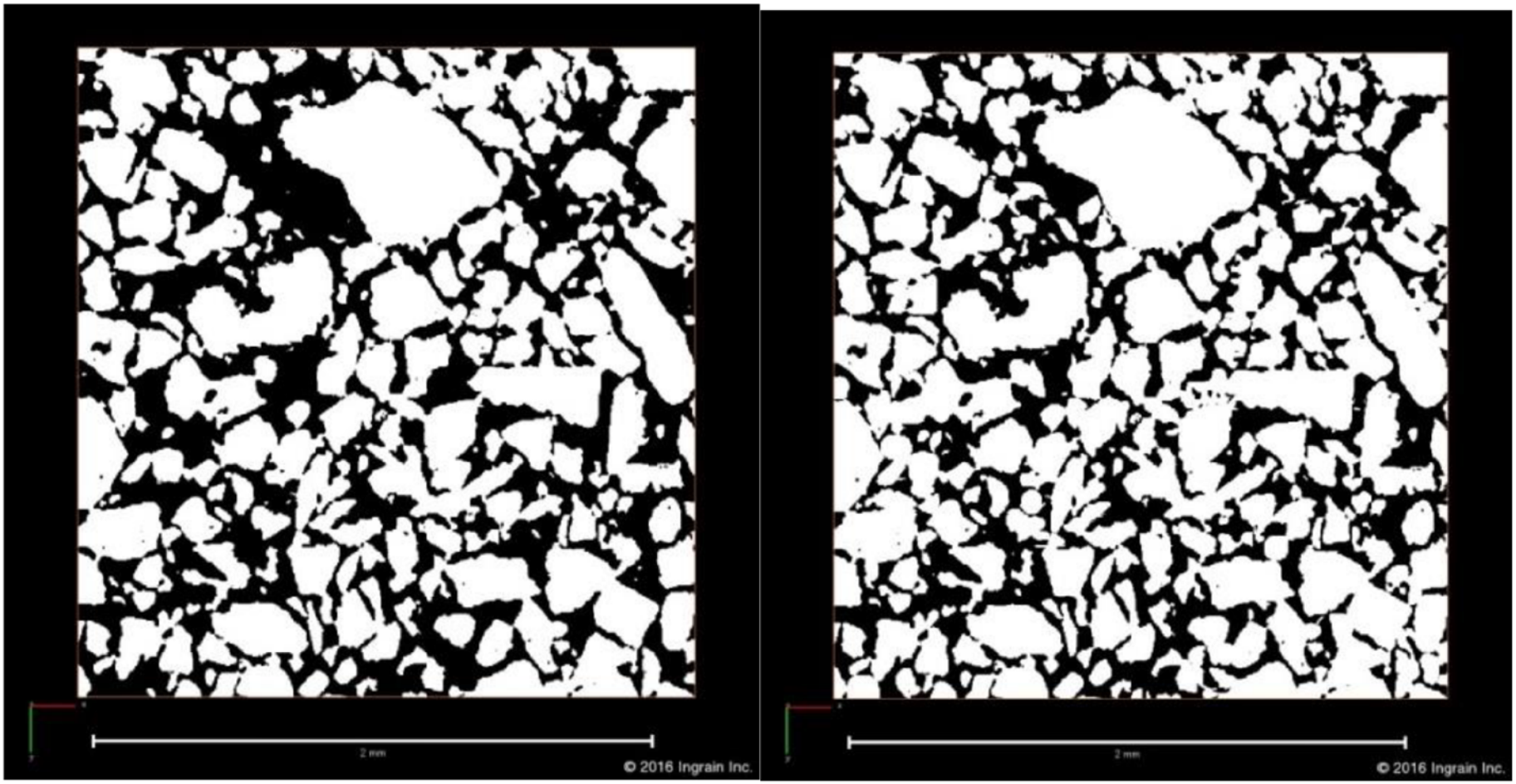

Figure 2. Plug 8-101 depth 2348.18 m sub-sample one single slice in axial view showing the digital pore and grain structure before (a) and after (b) digital conditioning.

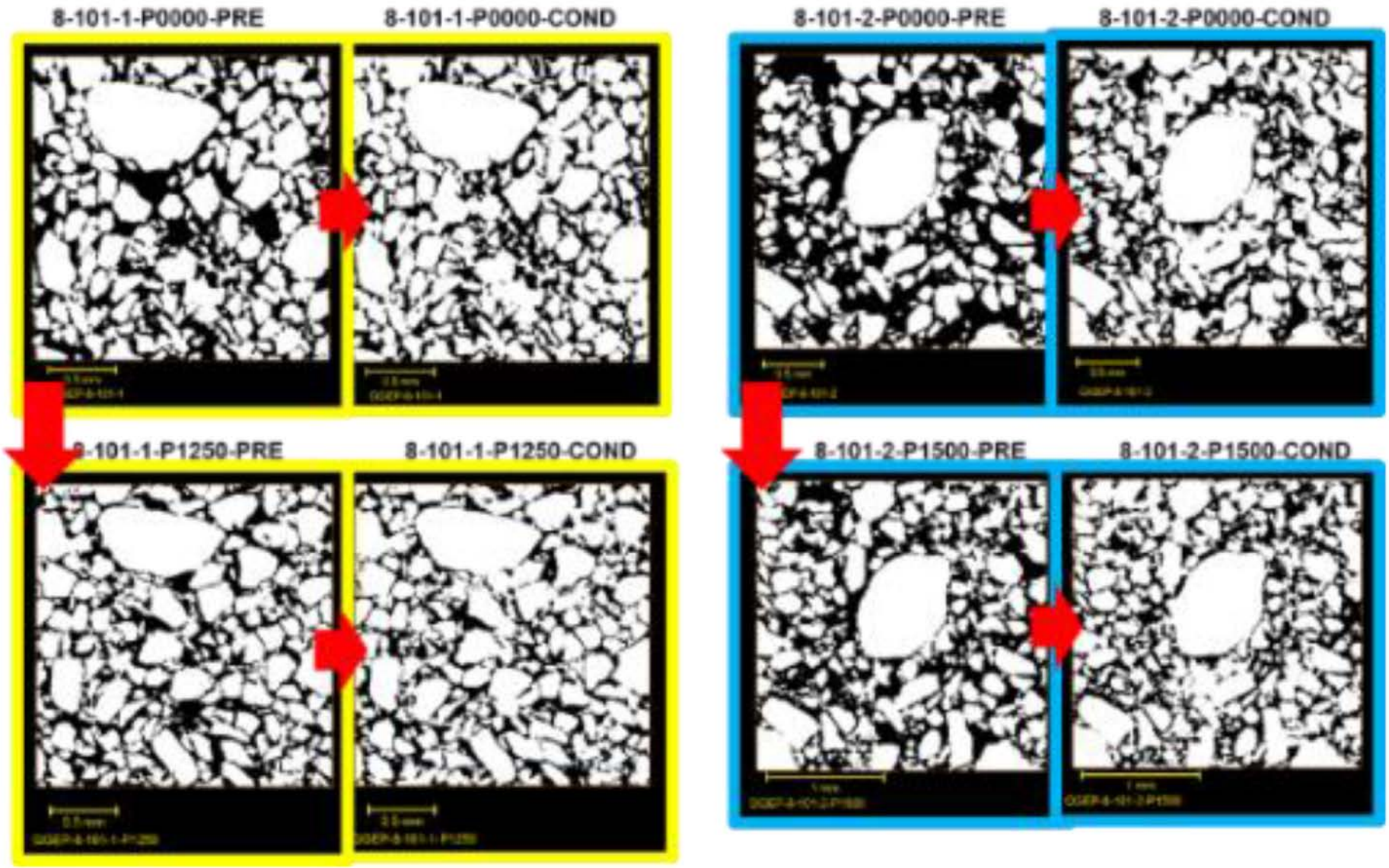

Figure 3. Comparison plug 8-101 depth 2348.18 m sub-sample 1 and 2 Low and high pressure before and after digital conditioning.

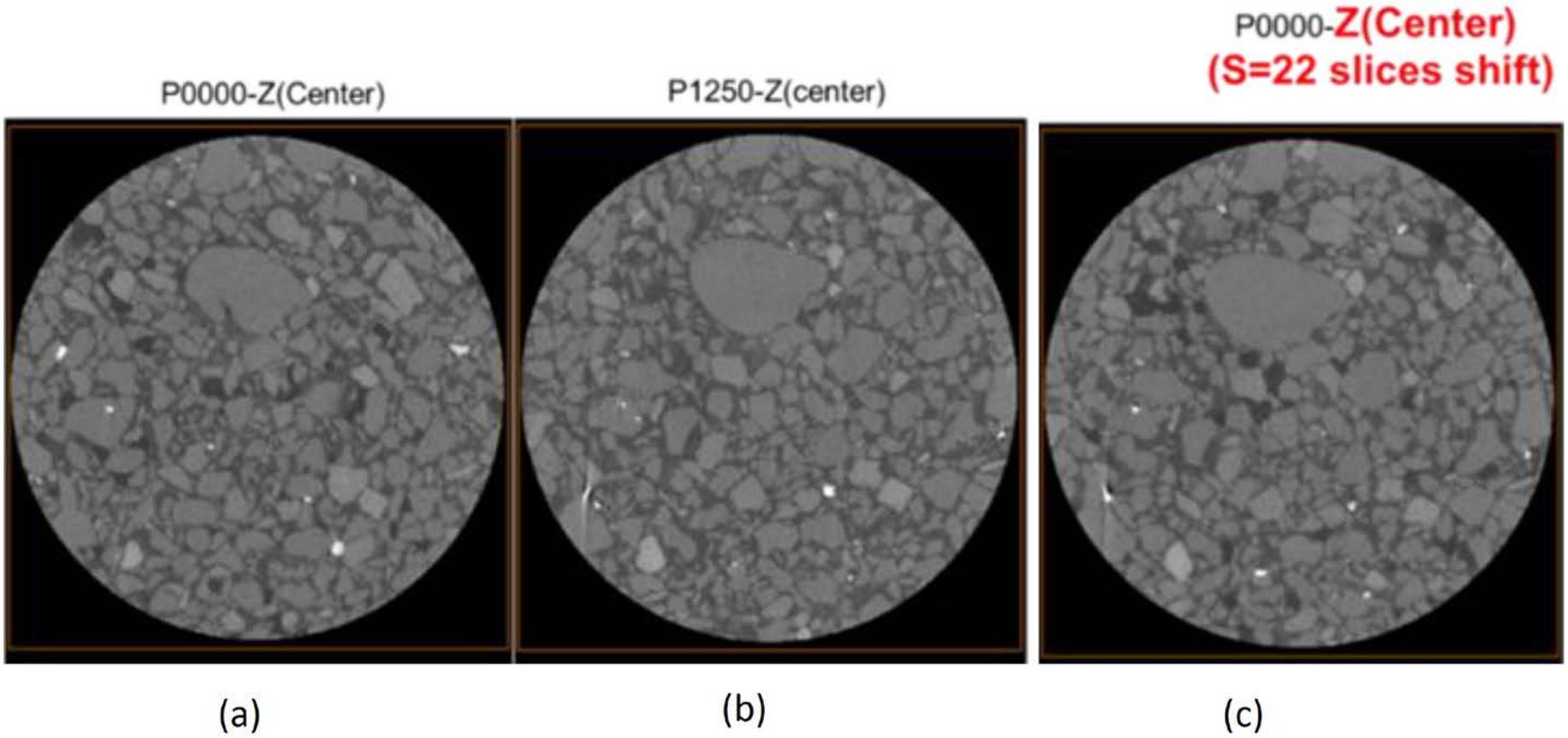

Figure 4. Sub-sample 8-101-1 depth 2348.18 m (a) PRE compression at low pressure at 20 psig, (b) POST compression at high pressure 1250 psig CT data at the same slice position on the XY direction indicating differences on the grain structure, (c) PRE compression at P0000 shift 22 slices above showing the same grain structure of (b).

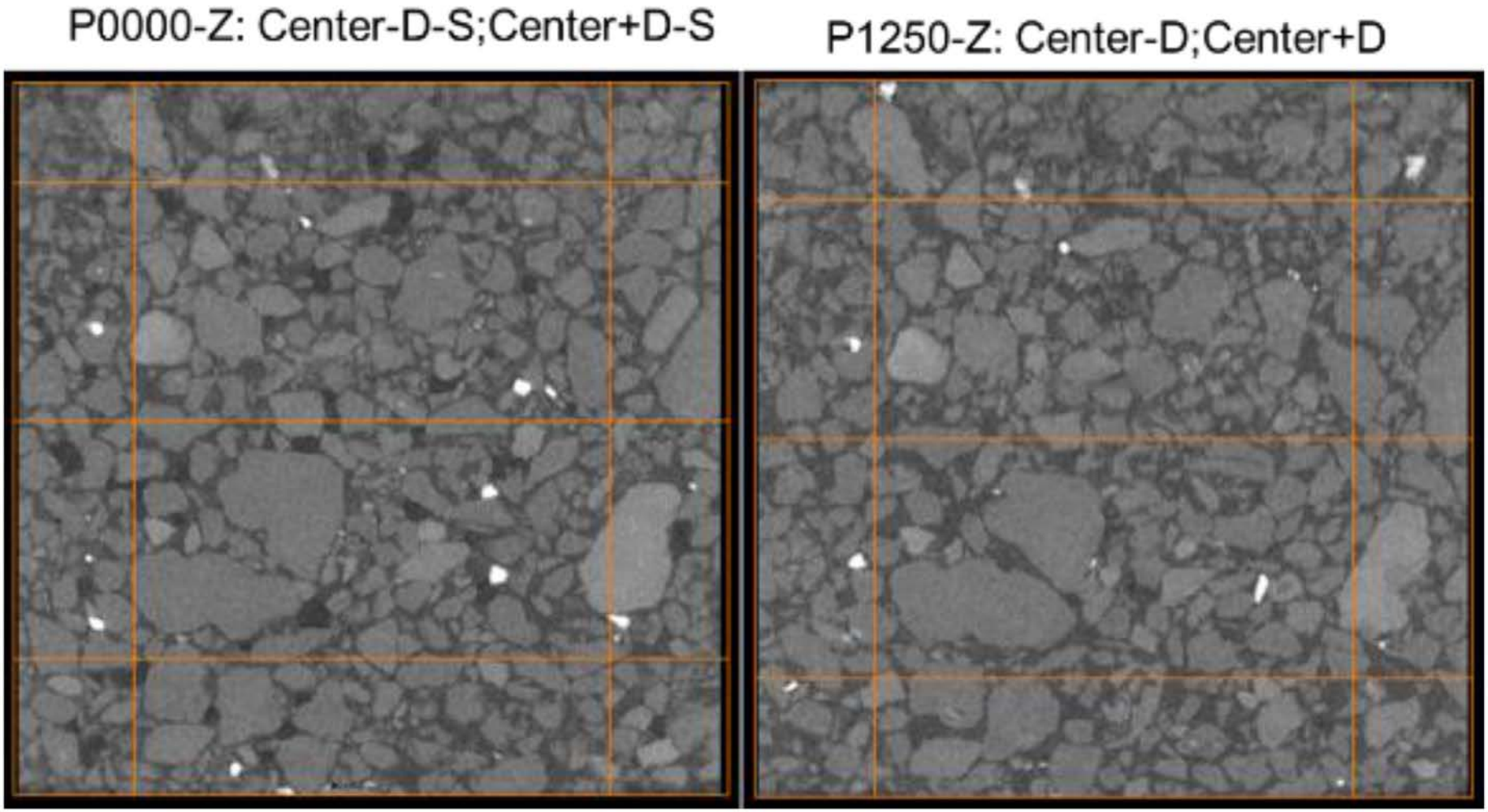

Figure 5. Sub-sample 8-101-1 depth 2348.18 m Pre- and Post- compression CT data on XZ view of the sub-sample, indicating a shift position on Z direction.

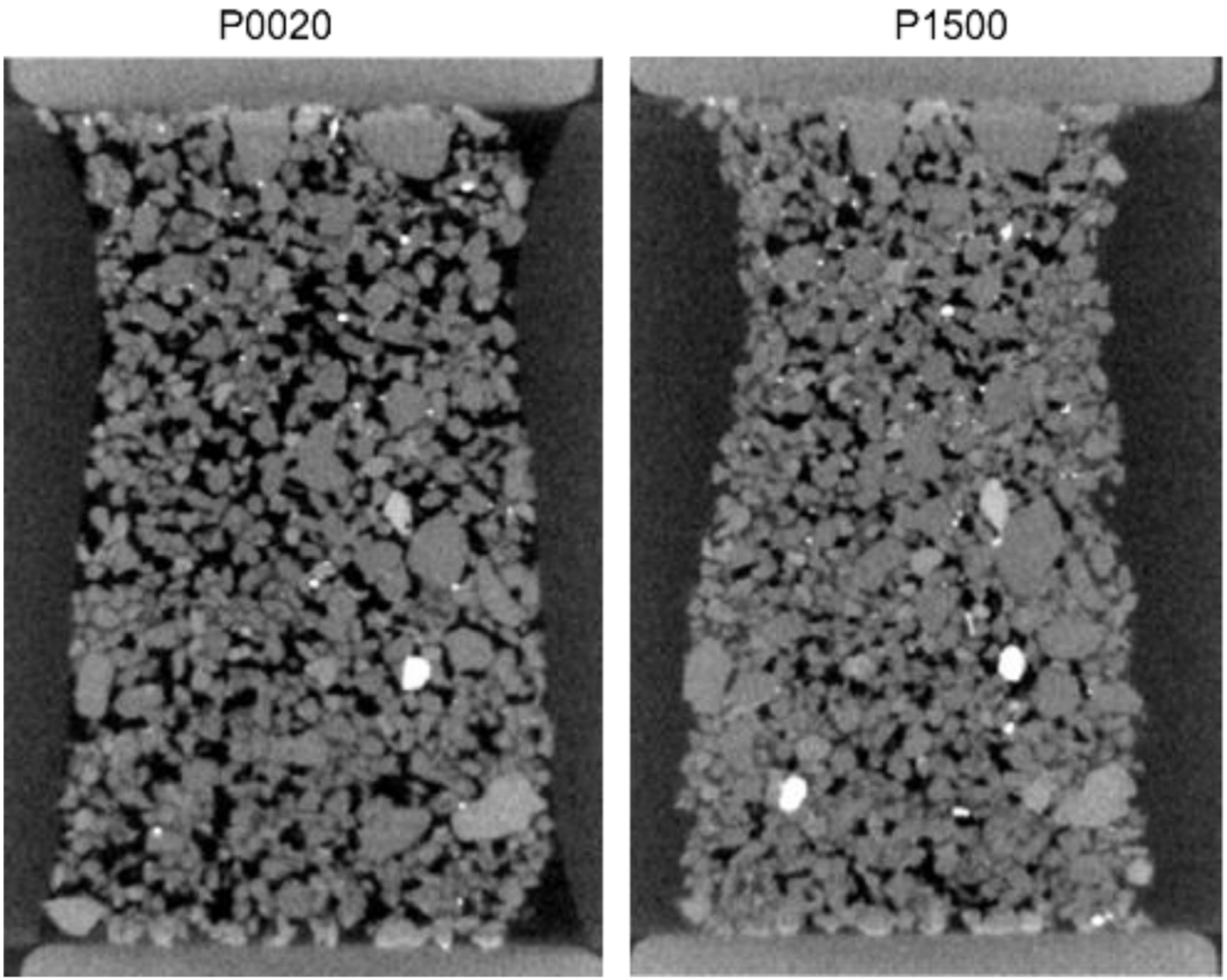

Figure 6. Single slice at two confining pressures: low (P0020) and high (P1500) pressure for sub-sample 4-3-2 depth 2375.85 m.

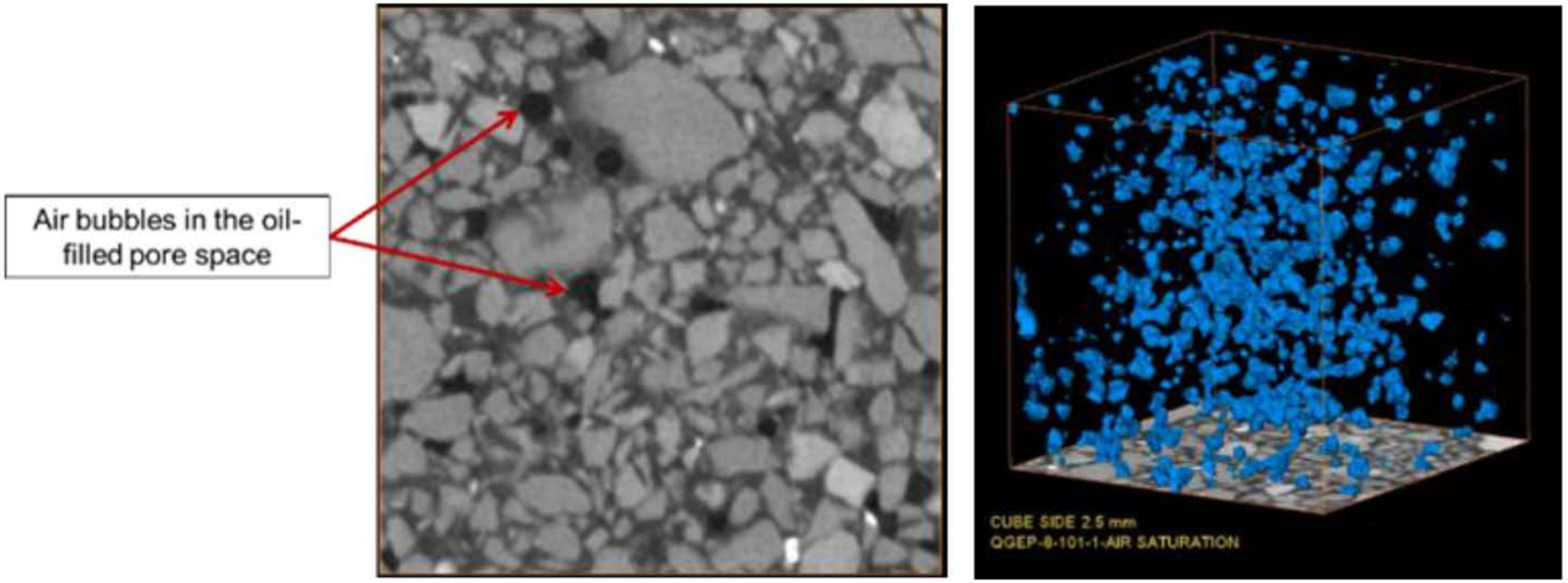

Figure 7. Single CT slice of sub-sample 8-101-1 depth 2348.18 m showing the air saturation during the compression process and a 3D perspective.

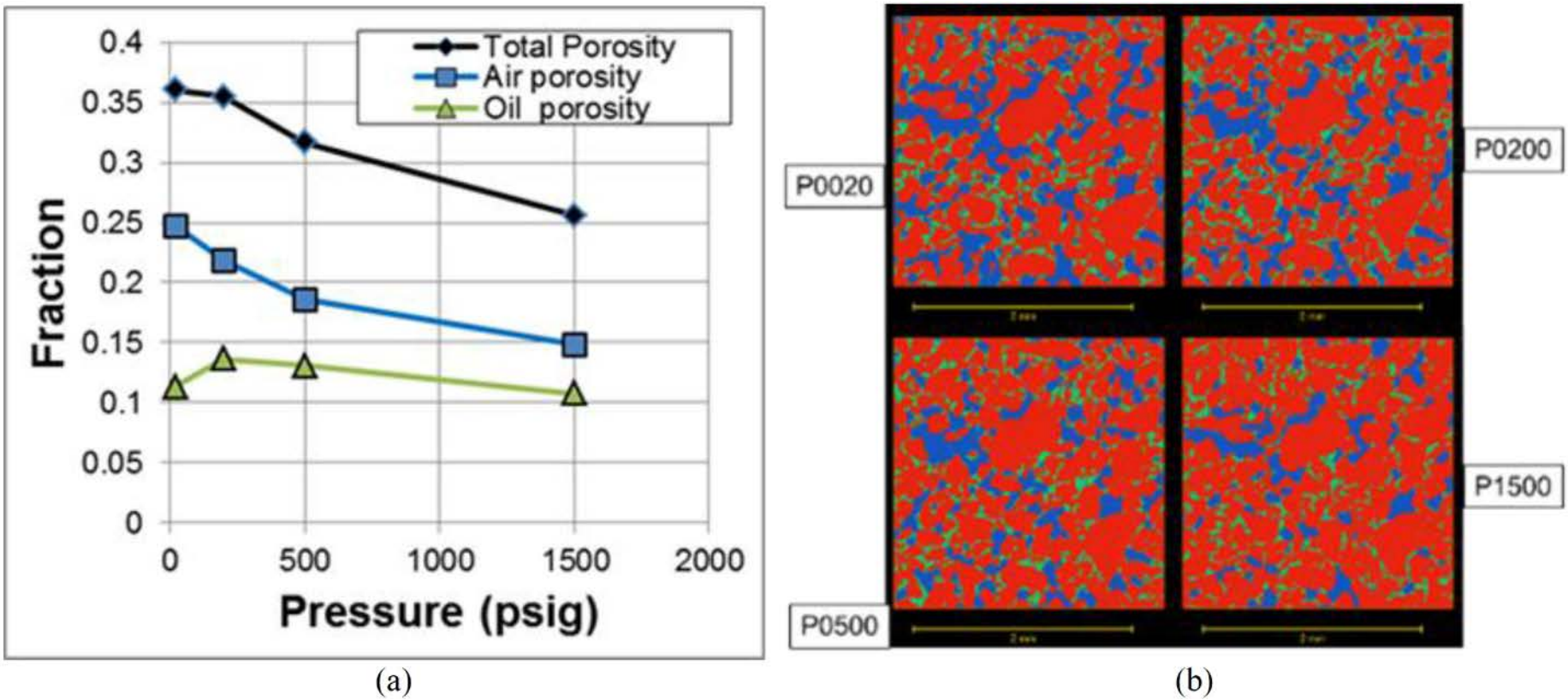

Figure 8. (a) Total porosity and air and oil fraction on the pore space for sub-sample 4-3-2 depth 2375.85 m in graphic mode compared with (b) CT segmented slice with grains in red, oil in green, and air in blue for sub-sample 4-3-2 depth 2375.85 m at four different pressures: 20, 200, 500, and 1,500 psig.

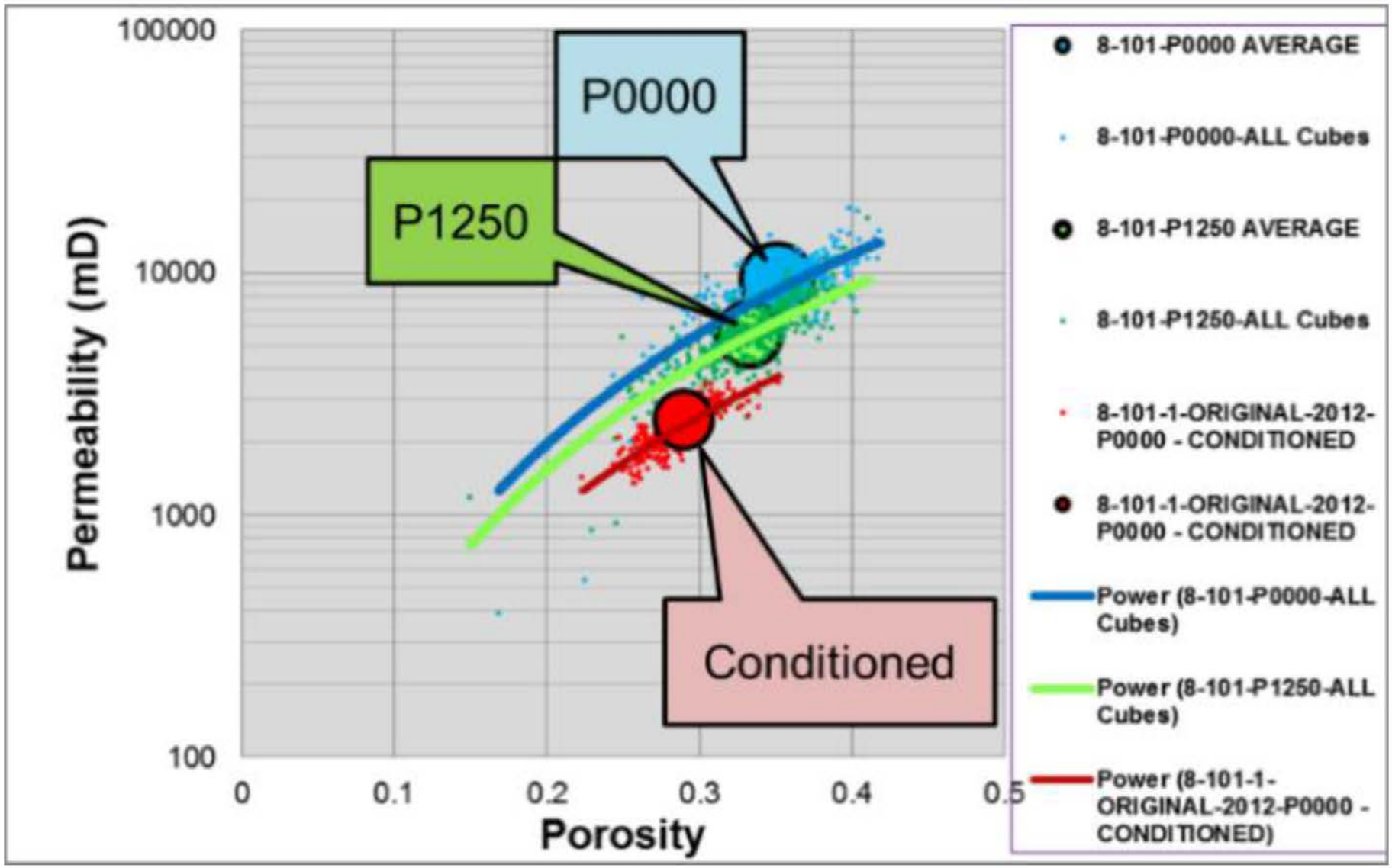

Figure 9. Example of processing of the PRE and POST hydrostatic compression CT data using digital conditioning and digital subdivision trend.

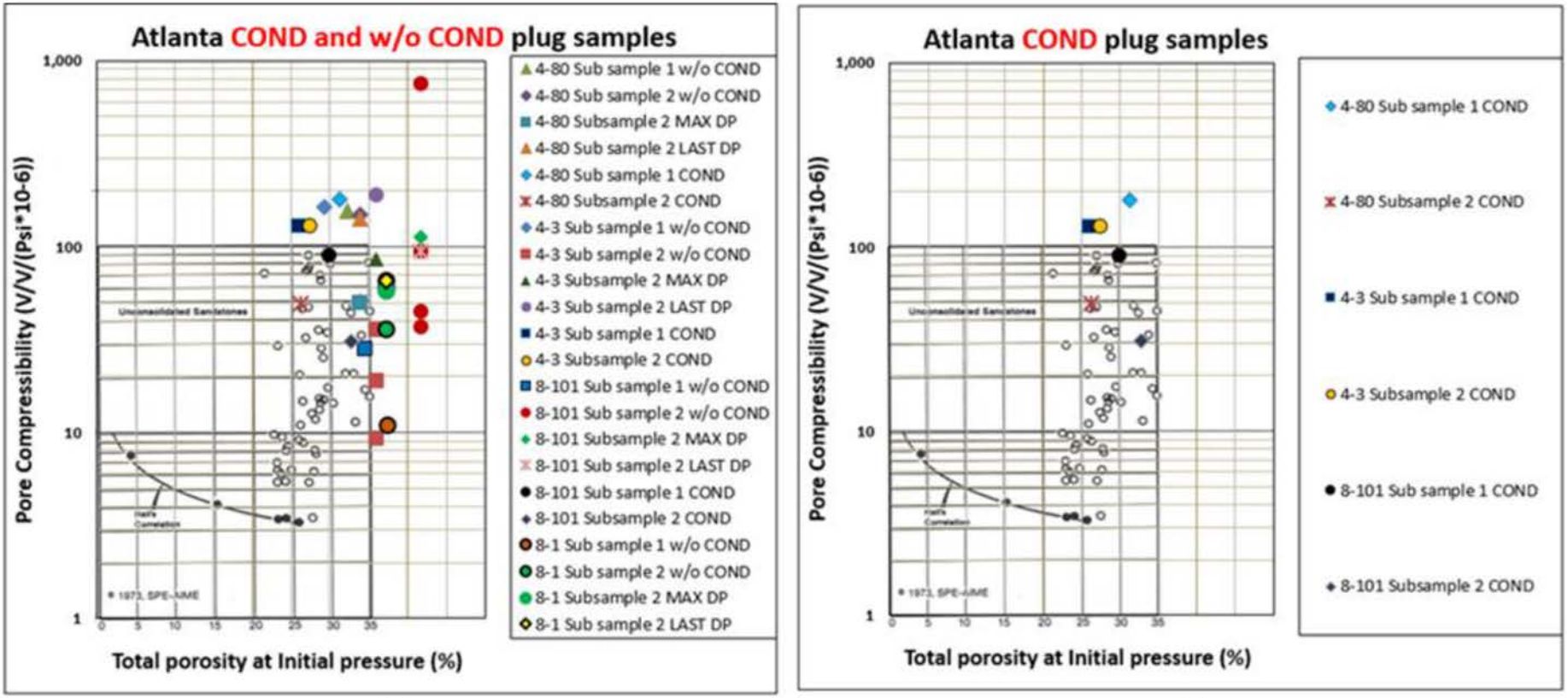

(a) (b)

Figure 10. Estimated compressibility for Atlanta sub-samples, including results before and after digital conditioning, superimposed on results reported by Newman (1973) for poorly consolidated samples: (a) Effective compressibility results before and after digital conditioning and (b) Effective compressibility results after digital conditioning.

Plug	Sub-sample	Depth (m)	Digital Conditioning	Resolution	Pixel Size (µm)	Low Pressure (psig)	High Pressure (psig)			
8-1	8-1-1	2323.43	NO	Micro4	4.12	20	-	-	1250	-
	8-1-2	2323.43	NO	Micro4	4.12	20	200	500	1500	2000
8-101	8-101-1	2348.18	YES	Micro4	4.12	20	-	-	1250	-
	8-101-2	2348.18	YES	Micro4	4.12	20	200	500	1500	2000
4-3	4-3-1	2375.85	YES	Micro4	4.12	20	-	-	1250	-
	4-3-2	2375.85	YES	Micro4	4.12	20	200	500	1500	-
4-80	4-80-1	2394.98	YES	Micro4	4.12	20	-	-	1250	-
	4-80-2	2394.98	YES	Micro4	4.12	20	200	500	1500	2000

Table 1. List of sub-samples under physical compression high and low pressure.

Pressure	Porosity	Air	Oil
4-3-P0020	0.361	0.247	0.114
4-3-P0200	0.355	0.218	0.136
4-3-P0500	0.317	0.186	0.131
4-3-P1500	0.256	0.148	0.107

Table 2. Total porosity and air and oil fraction on the pore space for sub-sample 4-3-2 depth 2375.85 m.

Plug	Depth (m)	Sub-sample		Porosity			Absolute Permeability (mD)		
			Pressure (psig)	TOTAL fraction	Connected fraction	Isolated fraction	X	Y	Z
8-1	2323.43	1	20	0.374	0.369	0.004	8324	9013	6312
		1	1250	0.369	0.368	0.002	8494	9493	6588
		2	20	0.372	0.372	0.000	6817	6928	6446
		2	1500	0.341	0.341	0.000	5097	5619	4839
8-101	2348.18	1	20	0.299	0.298	0.001	5678	5619	5128
		1	1250	0.299	0.299	0.000	5755	5329	5624
		2	20	0.328	0.328	0.000	8514	8265	7271
		2	1500	0.314	0.313	0.000	6076	6059	5927
4-3	2375.85	1	20	0.260	0.260	0.000	2514	2359	2093
		1	1250	0.219	0.219	0.000	1878	1910	1693
		2	20	0.274	0.274	0.000	4470	3913	4101
		2	1500	0.223	0.222	0.000	1954	1797	2071
4-80	2394.98	1	20	0.313	0.311	0.002	6158	6078	5266
		1	1250	0.244	0.244	0.000	2776	2743	2271
		2	20	0.262	0.262	0.000	2977	2907	2907
		2	1500	0.243	0.243	0.000	2373	2277	2178

Table 3. Summary of the total porosity and absolute permeability values achieved before and after hydrostatically compression CT.